Surface & Coatings Technology 203 (2009) 1457–1461

Contents lists available at ScienceDirect

Surface & Coatings Technology

journal homepage: www.elsevier.com/locate/surfcoat

Microstructure and properties of the compound layer obtained by pulsed plasma nitriding in steel gears

E.A. Ochoa [a], D. Wisnivesky [a], T. Minea [b], M. Ganciu [b], C. Tauziede [c], P. Chapon [c], F. Alvarez [a,b,*]

[a] Instituto de Física "Gleb Wataghin", Universidade Estadual de Campinas, Unicamp, 13083-970, Campinas, São Paulo, Brazil
[b] Laboratoire de Physique des Gaz et Plasmas (LPGP), UMR 8578, CNRS-Université Paris Sud, 91405 Orsay, France
[c] HORIBA Jobin Yvon S.A.S., 16-18 rue du canal, 91165 Longjumeau cedex, France

ARTICLE INFO

Article history:
Received 25 June 2008
Accepted in revised form 24 November 2008
Available online 6 December 2008

Keywords:
Plasma nitriding
Nitrides
Layered structure
Nano-hardness
Diffraction

ABSTRACT

The crystalline structure profile of the compound layer obtained by pulsed plasma nitriding in steel gears is reported. The nitrogen depth profile obtained by Radio Frequency Glow Discharge Optical Emission Spectroscopy is correlated with both the nano-hardness and the crystalline ε-Fe_3N/γ′-Fe_4N phases identified in the nitrided layer by X-ray diffraction. These results show the importance to control the nitriding parameters to avoid abrupt hardness changes along the case that can jeopardize the gear performance.

1. Introduction

Pulsed plasma nitriding is a thermo-chemical treatment applied mainly to iron alloys to improve fatigue strength, wear, and corrosion surface resistance. The formation of a compound layer ("white layer") provides a very hard surface as required in gears normally working at high speed. These applications require teeth with high root and flank stiffness to improve bending fatigue and low friction, the conditions to enable smooth running and wear resistance [1]. The relatively low temperature process (~540 °C) prevents dimensional distortion, eliminating post-machining work. What is more, the precise control of the compound layer properties makes the plasma nitriding process a valuable technique for these applications [2,3]. These benefits are attained through diffusion of nitrogen into the teeth gear surface and the formation of a white layer around 15–20 μm thick. In order to obtain a uniform white layer in gears presenting a different aspect ratio, specific conditions of pressure, current density, gaseous mixture, and temperature must be carefully determined [4]. Furthermore, depending on the nitrogen concentration, the compound layer may be constituted by ε-$Fe_{2-3}N$ or γ′-Fe_4N phases or a mixture of both. It is important to note that for some applications the formation of a homogeneous mono-phase is more desirable than a mixture of these crystalline structures of iron-nitrogen alloys [5]. This is because the different unit cell parameter of the cited crystalline phases can generate stress at the grain boundary, increasing the fragility of the layer. Indeed, in a recent work we have discussed the formation of a ε-Fe_3(N,C) hexagonal compact mono-phase crystalline phase by the addition of minute amounts of methane to the gaseous mixture constituting the plasma [6]. Also, the characteristics of the crystalline phases present in the compound layer obtained by different processes is important for other applications such as the hard coating deposited onto nitrided materials [7,8]. In summary, the formation of the ε-Fe_{2-3} N hexagonal mono-phase of 15–20 μm is important since it can prevent seizure and score in parts submitted to mechanical efforts [9].

In this study we have examined the properties of the compound layer in steel gears obtained by pulsed plasma nitriding in a production furnace by treating small lots of samples. The in-depth profile crystalline microstructure and the hardness of the compound layer were studied by X-ray diffraction (XRD) and nano-hardness, respectively. The evolution of these physical properties are analyzed and correlated with the material composition depth profile (1 μm resolution) obtained by Radio Frequency Glow Discharge Optical Emission Spectroscopy (RF GD-OES, GD-Profiler2 HORIBA, Jobin Yvon)) [10].

2. Experimental procedures

Teeth-shaped samples were manufactured from CK45 steel (%wt; C: 0.43-048, Si: 0.15-040, Mn: 0.4-0.50, P: max. 0.035, S: 0.020-0.040, Cr: 0.17-0.23, Ni: max. 0.25, Mo: max. 0.07, Al: 0.010-0, Fe: remainder), without any specific heat treatment. The core's nano-hardness of the material used for the study is ~4 GPa as measured by nano-hardness techniques. The shape and dimensions of the teeth are indicated in Fig. 1. A uniform plasma penetration depends on the recess of the teeth and it should be taken into account in establishing the experimental parameters giving a uniform compound layer [4].

* Corresponding author.
E-mail address: alvarez@ifi.unicamp.br (F. Alvarez).

0257-8972/$ – see front matter © 2008 Elsevier B.V. All rights reserved.
doi:10.1016/j.surfcoat.2008.11.025

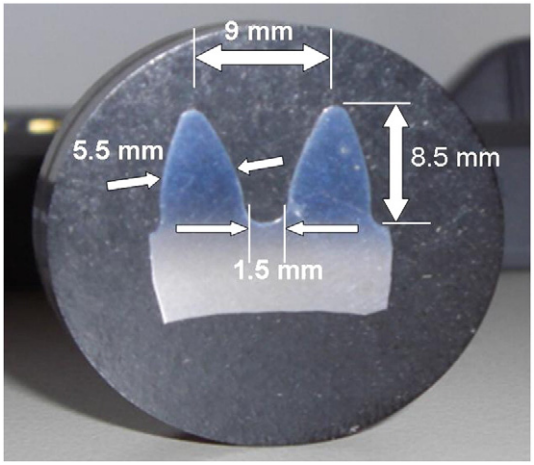

Fig. 1. Typical studied sample embedded in Bakelite and mirror polished. The main dimensions of the teeth are indicated.

Fifteen samples were studied and similar results obtained in all of them. Therefore, for the sake of simplicity, we shall report results obtained from a selected group of samples. The samples were nitrided at 540 °C in a commercial hot-wall, fully automatic *Plasmatec 450* pulsed plasma system, 120A/1000 V with capacity for 600 kg (*Plasma-LIITS*, 13083-970 Campinas, São Paulo, Brazil) [11]. In the present study we have performed the tests using small number of samples, i.e., using a small fraction of the furnace capacity. The samples were first cleaned with distilled water and neutral industrial detergent in an ultra-sonic bath. Afterward, the samples were rinsed with abundant distilled water. A gaseous mixture of $[N_2]/[N_2+H_2]=70\%$ was used along the four-hour nitriding process at ~4 Torr chamber pressure. Here, the square brackets indicate flux in sccm (standard cubic centimeters per minute). The system takes 2 h to reach the working temperature. After finishing the treatment, the remaining gaseous mixture used during the nitriding is evacuated to the background system pressure (<0.02 Torr). Immediately, the furnace is filled up with pure N_2 (99.999%) up to 400 Torr. The furnace is opened after ~4 h, i.e., when the temperature is reached around 80–100 °C.

Table 1 shows the complete set of parameters used in the nitriding process giving the best results. The main parameters controlling the process are current density, gaseous mixture, and temperature. Also, in order to obtain good results cleaning the surface is very important. Therefore, 1 h before starting the nitriding plasma and during the heating process, the samples were sputtered using argon-hydrogen plasma (~90% Ar in H_2). This procedure proved important to guarantee the white layer formation [12].

The hardness profile of the samples was measured by nano-indentation (Nano-Test 300, Microtech) on cross-sections slices obtained from the gears and the data analyzed by the Oliver-Pharr method [13]. Since the white layer is very thin, the use of a nano-indentator is mandatory to obtain a worthy hardness profile. The nano-hardness measurements were not corrected by piling up effects. We remark that the hardness preferred units in technological applications are HV. However, the nano-hardness is normally giving in GPa since there is not a consensus about the equivalence between the two scales. Roughly speaking 1 GPa ≅ 100 HV could be considered, but it is strongly dependent on the load used, depth, imprint size, etc [14]. Nevertheless, this equivalence must be taken carefully. Indeed, the core hardness of the used steel comes out to be ~400 GPa and 280 HV0.05 by using the nano-test or micro hardness techniques, respectively. Information regarding the in-depth crystalline structure was obtained from X-ray measurements. The apparatus used in this measurement is a Shimadzu, LAB X-XRD-6000 in a Bragg-Brentano X-ray diffraction configuration using the CuKα monochromatic line. The optical study (Olympus BX41M) of the compound layer was obtained by the usual procedure of bakelite mounting, polishing (diamond powder 1 μm mesh), and Nital room temperature attack (2% v/v nitric acid in absolute ethanol). The in-depth crystalline evolution of the compound layer was obtained by successively polishing each sample step by step and obtaining a X-ray difractogram in each step. The polishing process in each step was performed using 1 μ mesh diamond powder (Stuers, Tegrapol-11, 300 rpm). In order to minimize polishing effects on the nano-hardness measurements the following precautions were taken: 1) the polishing procedure used in the experiment was as mild as possible; 2) the hardness of the nitrided layer is in general much larger than the extra hardness introduced by polishing; and 3) the polishing procedure is maintained the same as much as possible. In this way we can do relative hardness comparison. Finally, to reduce errors on the in depth profile analysis, the XRD spectra were taken locating the sample at the same position and incidence X-ray angle giving ~1 μm radiation penetration. The crystalline structure determined by this procedure is compared with the depth profile composition obtained from RF-GD-OES quantitative analysis.

Table 1
Nitriding parameters

Chamber pressure	Current* density	Process temp.	Pulse on	Pulse off	Voltage	$N_2/[N_2+H_2]$	Process time	Compound thickness
(Torr)	(mA/cm^2)	(C^0)	(μs)	(μs)	(V)	(%)	(h)	(μm)
4.0	~0.8	540	50	150	500	70	4.0	15

*Estimated (see Appendix A).

3. Results and discussion

3.1. Compound layer uniformity

As remarked in the Introduction, the plasma conditions are decisive for the uniformity of the white layer [4]. This is so because the plasma penetration in a deep recess depends on a complicated interaction of working pressure, voltage, current density, gaseous mixture, pulsed frequency, and temperature. As a rule of thumb, increasing pressure and current will make the plasma penetrate deeper into the recesses [15]. Regarding the current and neglecting secondary electrons ejected from the surfaces, the current collected by the gears is basically formed by N_2^+ and H_2^+ ions. Excess of current leads to overheating, power losses, non-uniform thickness, and formation of cracks in the layer. Therefore, for production scaling purpose it is important to know the density of current needed in the process. However, current measurements are very difficult to accomplish since sharp edges tend to drag more current than smooth surfaces and only average current densities are obtained. An indirect procedure to estimate the actual current density at the gear teeth is reported in the Appendix A. Using this approach, we have obtained a current density of ions of ~0.8 mA/cm^2. Another important phenomenon to be considered is the hollow cathode glow discharge regime occurring in small holes. The shape and size of the small holes can abnormally increase the electron density, augmenting locally the ion bombardment [4]. Therefore, overheating and/or excess current density can jeopardize the uniformity and the quality of the compound layer. All these considerations must be taken into account in selecting the working conditions. Table 1 summarizes the best set of parameters found in this work. These conditions provide quite homogeneously nitrided layers, compact, and uniform as the example shown in Fig. 2. Moreover, Fig. 3 shows details of the teeth tip of the nitrided layer of one of the studied samples. The ~12 μm thick layer covering the teeth shows a quite uniform compound case matching the sample profile (Fig. 3a). This uniformity stresses the importance of the material surface finishing on the formation of a uniform compound case. Indeed, tiny surface oscillations remaining from the gear fabrication

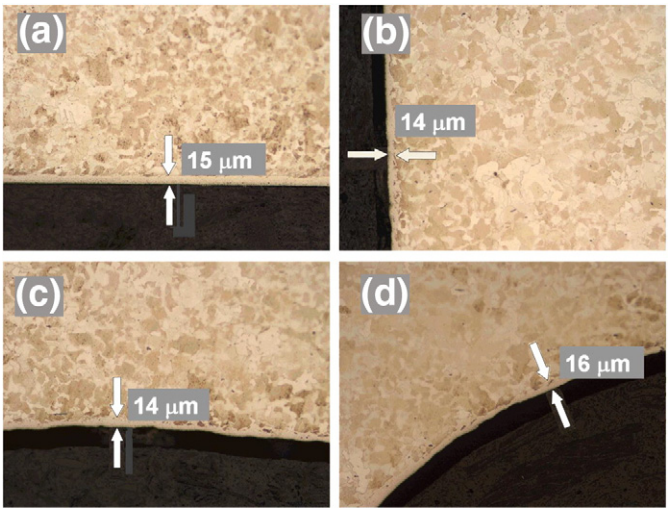

Fig. 2. (a) and (b) Nitrided layer at the top and flank part of the teeth, respectively; (c) and (d) Nitrided layer details in two different regions of the bottom part of the teeth shown in Fig. 1.

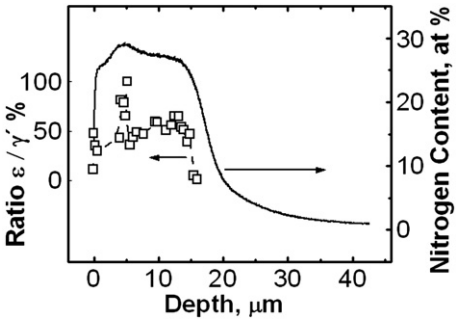

Fig. 4. Nitrogen and percentage of the ε-$Fe_{2\text{-}3}N$/γ′-Fe4N ratio profiles. The ε/γ′ ratio was obtained by integrating the corresponding bands associate to each phase from the in-depth diffractograms (Fig. 5).

procedure are perfectly matched (up to fractions of microns) by the compound layer even in the case of thicker nitrided layers (Fig. 3b). Moreover, some porosity can be observed at the surface of the layer. However, in this work we have not investigated specifically the porosity and its influence on the performance of the nitrided layer needs to be further studied.

3.2. Nitrided layer composition

Fig. 4 (right axis) shows the compound layer composition obtained by the RF-GD-OES technique. The maximum nitrogen concentration (left axis) observed near the sample surface can be explained by the following two reasons. First, at the working pressure reported here, most of the nitrogen atoms are implanted in a few atomic layers below the material surface (~4 nm) [16]. Second, and more important, when the process ends, the nitrogen supply stops and the slow furnace cooling down process allows N back diffusing into the furnace chamber, i.e., a denitring process takes place due to the abrupt nitrogen concentration gradient relative to the free surface. Also, the relatively low N diffusion coefficient in the nitrided layer prevents important further penetration of N in the material bulk. The long nitrogen concentration tail observed deeper in the material suggests a diffusion controlled process [17]. Nevertheless, some influence from knock head atoms into the sample during the GD-OES measurements can be contributing to the observed nitrogen profile. However, the hardness profile performed on samples previously to GD-OES measurements shows a similar long tail that the N concentration profiles. Considering that in general there is proportionality between nitrogen concentration and hardness, one can conclude that the knock head effect is probably negligible [25].

We note, finally, that the left axis in Fig. 4 represents the in-depth ratio of the areas under the X-ray main reflection bands associated with the ε-$Fe_{2\text{-}3}N$ and γ′-Fe_4N crystalline species constituting the compound layer. This subject will be further discussed in Section 3.3 [18].

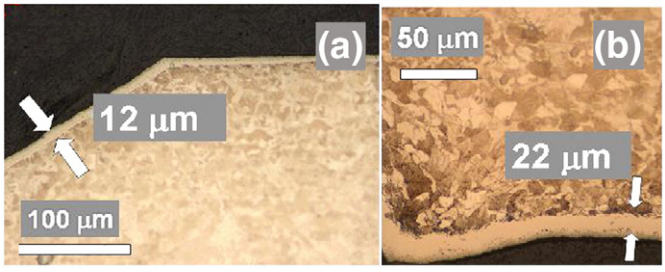

Fig. 3. a) Micrograph of the sample displayed in Fig. 1 showing the detail of the compound layer at the tip of the gear teeth. b) Micrograph of another sample showing a thicker compound layer matching the wavy surface profile of the gear. The grain boundaries of the material core are also visible. The compound layer was revealed by attacking the surface with Nital solution (2% v/v nitric acid in absolute ethanol).

3.3. Compound layer: crystalline phases and composition

The in-depth nitrogen concentration is correlated to the crystalline structure of the compound layer (Fig. 5a,b). For clarity reasons, two plots are displayed with a selected number of diffractograms. As previously mentioned, the case is formed by a mixture of the ε-$Fe_{2\text{-}3}N$ and γ′-Fe_4N iron nitride phases and the α phase of the base material. These phases hold reflections located at 2Θ ~45 and 83% for α(110) and α(211), respectively. Also, at 2Θ ~43 and 85% are reflections associated with ε(101) and γ′(311), respectively [19–21]. Additional reflections related with these phases reported by other authors are not present in our difractrogram, a fact that might be due to the type of studied samples [22]. As observed in Fig. 5, the γ′-Fe_4N and ε-$Fe_{2\text{-}3}N$ phases are diminishing along the compound layer while the α phase increases. Indeed, at a depth of ~20 μm, the presence of the nitrides phases ε-$Fe_{2\text{-}3}N$ and γ′-Fe_4N are negligible indicating that nitrogen is incorporated in the matrix of the α phase. The relative evolution associated with the nitrides phases in the compound layer are summarized in Fig. 4, left axis. The plot represents the ratio of the areas of the peaks associated with the X-ray reflections corresponding to the ε-$Fe_{2\text{-}3}N$ and γ′-Fe_4N crystalline phases as a function of the compound layer depth. The phases constituting the compound layer were identified by taking X-ray difractograms at several depths. In order to do this, the sample was polished and a difractrogram obtained by successively repeating this procedure step by step (Section 2) [18]. This plot tells us about the relative importance of the crystalline phases present in the compound layer as a function of depth and nitrogen concentration. The uncertainty of the experimental data is of the order of the size of the dots. The curve shows a small increase of the nitrogen richer phase (ε-$Fe_{2\text{-}3}$ N) around ~5 μm, consistent with the nitrogen concentration profile. Afterward, the ratio stabilizes, suggesting a constant white layer phase composition contributing to avoid seizure and score in the treated material [9,23]. Finally, we remark that the measured amount of N by GD-OES includes all the atoms in the layer and part of it is forming disperse fine metallic nitrides with the allowing components of the steel, i.e., the total measured N atoms are not all incorporated in the ε-$Fe_{2\text{-}3}N$ and γ′-Fe_4N phases.

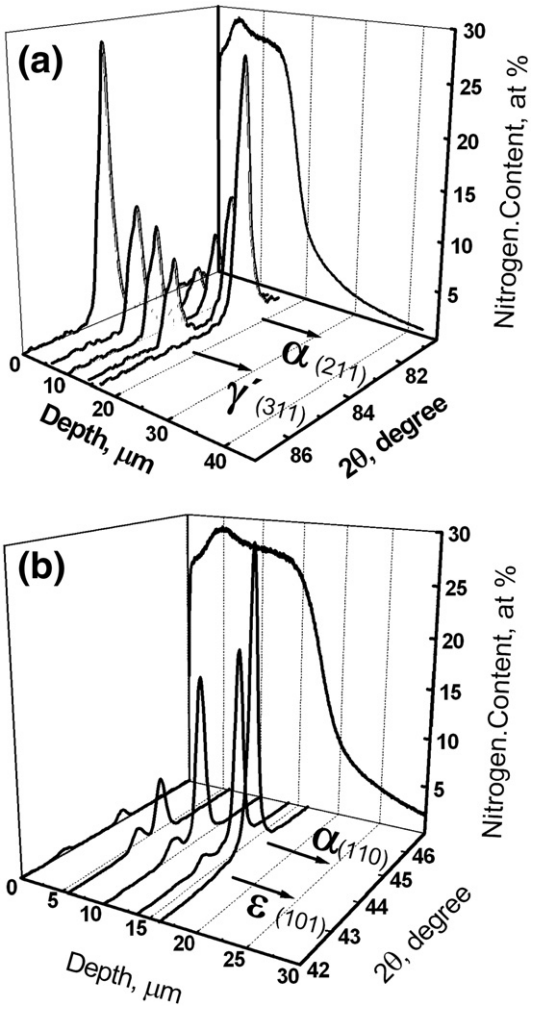

Fig. 5. Comparison of the in depth evolution of the diffractogram and nitrogen concentration (right wall) corresponding to the compound layer of the sample displayed in Fig. 2a. For the sake of clarity the diffractogram is divided in reflections associates with the γ′, α (a) and ε, α (b) crystalline phases. For clarity reasons, only a selected number of diffractograms are displayed.

3.4. Hardness and composition profiles

Fig. 6 shows the nitrogen, iron and nano-hardness profiles of one of the studied samples as a function of depth. As observed, the compound layer extends up to ~20 μm and the hardness reaches the core value at ~35 μm. We remark that a relatively long nitrogen diffusion tail diminishes the stress generated by abrupt hardness variations [24]. Fig. 7 shows the hardness vs. nitrogen concentration

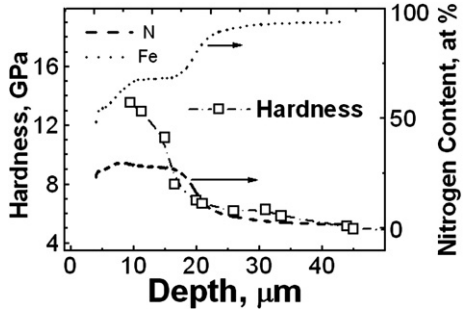

Fig. 6. Open squares: nano-hardness vs. nitrogen concentration profile. Solid and dashed curves: nitrogen and iron concentration profiles for the same sample studied in Fig. 4. The hardness experimental error is of the order of the symbols.

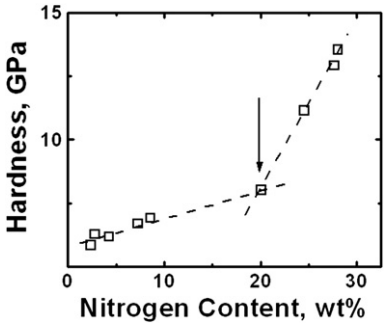

Fig. 7. Hardness vs. nitrogen concentration obtained from Fig. 6. The arrow indicated a change in the crystalline structure (vide Fig. 5).

obtained from Fig. 6. This plot shows two regions of a quite good proportionality between hardness and nitrogen concentration [25]. The breaking in the slope at around 20 at.% nitrogen concentration reflects the structure changes of compound layer crystalline. Indeed, Fig. 5 shows that around this nitrogen concentration the ε-$Fe_{2-3}N$ and γ′-Fe_4N phases are disappearing and the remaining nitrogen is included in the α crystalline phase.

4. Conclusion

A comprehensive study on the properties of the compound layer obtained by pulsed plasma in a gear steel (CK45) is reported. The X-ray diffractograms show that the ε and γ′ nitrides phases form the compound layer. Due to the cooling down process, the ε/γ′ ratio increases in a narrow region near the material surface (~5 μm). The lack of homogeneity can induce stress in the nitrided case and more work is needed to diminish this effect by adjusting the nitriding parameters.

A correlation between nitrogen concentration and hardness was found along the compound layer. The evolution from ε, γ′ to α phase containing nitrogen along the compound layer was mapped by X-ray diffractograms. This transformation is accompanied by a relatively abrupt slope change in the hardness vs. nitrogen concentration profile. This result could cause extra stress of the nitrided layer and should be considered when choosing the parameter's process. Finally, a quite uniform thickness compound layer along the teeth profile is obtained through an adequate choice of the deposition parameters, such as pressure, current density, gaseous mixture, and temperature.

Acknowledgments

This work was partially sponsored by Fapesp, Project 05/53926-1. EAO and FA are FAPESP (07/50483-7) and CNPq fellows, respectively. FA is indebted to the LPGP, CNRS-Université Paris Sud, Orsay, for their support during his sojourn in France. The authors are indebted to C. Piacenti for helping with the experiments.

Appendix A

In order to estimate the current density on the nitrided sample, we start considering the amount of nitrogen incorporated in a compound slab of 1 cm^2 cross section and 15 μm depths, i.e., ~1.5×10^{-3} cm^3. The amount of nitrogen atoms in the slab is related to the current density by $J \cong 4q\beta n/(\gamma t)$, where γ is the sticking factor assumed to be one; t is the process time, n the number of N atoms in the slab, and q the electronic charge. The factor β is related to the ionization efficiency of the gases used in the process. The coefficient 4 comes from the current duty cycle (see Table 1).

The average stoichiometry of the compound layer can be estimated by the ratio between the N and Fe at.% integrated areas of the concentration curves displayed in Fig. 6, i.e., ~0.35. In this approximation

we have assumed that nitrogen is mostly forming iron nitrides compounds. So, an average stoichiometry near to $Fe_{2.8}$ N is obtained. Therefore, the average molecular mass is $<\mu>=2.8\ \mu(Fe)+\mu(N)\cong 169.6$. Considering an average density of the nitriding iron phases of ~6.35 g/cm^3, the number of particles per cubic centimeter contained in a molar mass of compound layer is $\sim 2.2\times 10^{22}$ particles/cm^3. Thus, the total number of nitrogen atom in a compound layer slab of $\sim 1.5\times 10^{-3}$ cm^3 volume is $\sim 3.3\times 10^{19}$. Assuming that all the N_2^+ projectiles are dissociated upon collisions [26], the net charge contribution to the current must be considered half of the incorporated nitrogen atoms in the slab, i.e. $n\cong 1.7\times 10^{19}$. The factor β depends on the gases relative ionization cross section $r=\sigma(H_2)/\sigma(N_2)$, i.e., the amount of ion nitrogen contributing to the current has to be weighted by the ionization cross sections and the mixture composition. The maximum cross section σ can be estimated by using the Thompson classical approximation $\sigma\cong \upsilon\pi(q/4\pi\varepsilon_0)\ 1/E^2{}_i$, where ε_0 is the vacuum permittivity, υ is the valence number of electrons, and *Ei* is the gas ionization energy [27]. Then, $r\cong 0.23$ and the effective number of ions $I^+=(N_2^+ + H_2^+)$ arriving to the sample is proportional to the total gaseous flux Φ weighted by the ionization cross section and gaseous mixture composition (70% nitrogen and 30% hydrogen):

$$I^+ \sim \sigma(N_2)0.7\Phi + \sigma(H_2)0.3\Phi = \sigma(N_2)[0.7\Phi + 0.3\,r\,\Phi]$$
$$= \sigma(N_2)[0.7\Phi + 0.069\,\Phi].$$

The first (second) term in the bracket is the actual N_2^+ (H_2^+) contribution to the total number of ions ($I^+\sim 0.769\Phi$) arriving to the surface sample, i.e., 0.91 and 0.09 for N_2^+ and H_2^+ ions, respectively. Thus, only ~91% of the ionic current comes from nitrogen contribution; i.e., the current J is overestimated by 9% and $\beta\cong 1.09$. Substituting in the expression for the current for a 4 h process, $J\cong 4q\,\beta\,n/(\gamma\,t)$~0.8 mA/cm^2. We close this section commenting that a sticking factor around one considered in this estimation is consistent with both low energy [28] ions impinging the sample and low current density [19,29]. Low energy ions guarantee negligible nitrogen sputtering and low current density (small covering ratio) increasing nitrogen reaction probability to ~100%, i.e., sticking factor near to one.

References

[1] M. Boniardi, F. D`Errico, C. Tagliabue, Eng. Fail. Anal. 13 (2006) 312.
[2] L. Chiu, C. Wu, H. Chang, Wear 253 (2002) 778.
[3] P. Psyllaki, G. Kefalonikas, G. Pantazopoulos, S. Antoniou, J. Sideris, Surf. Coat. Technol. 162 (2002) 67.
[4] Yong M. Kim, Jeon G. Han, Surf. Coat. Technol. 171 (2003) 205.
[5] Y.H. Qiang, S.R. Ge, Q.J. Xue, J. Mater. Process. Technol. 101 (2000) 180.
[6] R.L.O. Basso, R. Candal, C.A. Figueroa, D. Wisnivesky, F. Alvarez, Surf. Coat. Technol. 203 (2009) 1293, doi:10.1016/j.surfcoat.2008.10.006.
[7] D. Braga, J.P. Dias, A. Cavaleiro, Surf. Coat. Technol. (2006) 4861.
[8] A. Chala, C. Nouveau, M.A. Djouadi, P. Steyer, J.P. Millet, C. Saied, M.S. Aida, M. Lambertin, Surf. Coat. Technol. 200 (2006) 6568.
[9] T. Bell, Y. Sun, A. Suhadi, Vacuum 59 (2000) 14.
[10] See for instance, Glow Discharge Optical Emission Spectroscopy (Rsc Analytical Spectroscopy Monographs) by T. Nils and R. Payling. Editor: N. Barnett. The Royal Society of Chemistry, Athenaum Press Ltd., Gateshead, Tyne and Wear, UK (2003).
[11] L.F. Zagonel, C.A. Figueroa, R. Droppa Jr., F. Alvarez, Surf. Coat. Technol. 201 (2006) 452.
[12] C.A. Figueroa, S. Weber, T. Czerwiec, F. Alvarez, Sripta Materialia 54 (2006) 1335.
[13] W.C. Oliver, G.M. Pharr, J. Mater. Res. 7 (1993) 1564.
[14] See for instance J. Malzbender, J. of European Ceramic Society, 23, 1355 (2003); K. Abdu Al-Rub, Mech. of Mat., 39, 787 (2007).
[15] See for instance, B. Chapman, Glow Discharge Processes, Wiley-Interscience Publications, 1980.
[16] C.A. Figueroa, E. Ochoa, F. Alvarez, J. Appl. Phys. 94 (2003) 2242.
[17] See for instance, Materials Science and Engineering: An Introduction, William D. Callister, Willey, 2006.
[18] A. Medina-Flores, J. Oseguera, P. Santiago, J.A. Ascencio, Surf. Coat. Technol. 188 (2004) 7.
[19] L.F. Zagone, E.J. Mittemeijer, F. Alvarez, Mat. Sc. & Tecn. (in press), doi:10.1179/174328408X332780.
[20] A. Medina-Flore, J. Oseguera, P. Santiago, J.A. Ascencio, Surf. Coat. Technol. 188–189 (2004) 7.
[21] L.F. Zagonel, F. Alvarez, Mater. Sci. Eng. A 465 (2007) 194.
[22] M.A.J. Somers, B.J. Kooi, L. Maldzinski, E.J. Mittemeijer, A.A. Van den Horst, A.M. Van der Kraan, N.M. Van der Pers, Acta Mater. 5 (1997) 2013.
[23] R.L.O. Basso, C.A. Figueroa, L.F. Zagonel, H.O. Pastore, D. Wisnivesky, F. Alvarez, Plasma Process Polym. 4 (2007) S728.
[24] S. Timoshenko, J. Opt. Soc. (1925) 233.
[25] E.A. Ochoa, C.A. Figueroa, F. Alvarez, Surf. Coat. Technol. 200 (2005) 2165.
[26] H.K. Hu, J.W. Rabalais, J. Chem. 85 (1981) 2459.
[27] See for instance, Principles of Plasma Discharge and Materials Processing, by M.A. Liberman and A.J. Lichtenberg, Wiley-Interscience Publication, New York, 1994.
[28] In the experimental conditions used in this work (500 V and 4.0 Torr) the energy of the ions (H_2^+ and N_2^+) impinging the gears due to inelastic scattering losses is E~50 eV. See R. Wei, Surf. Coat. Technol. 83, 218 (1996).
[29] H. Winters, J. Chem. Phys. 44 (1966) 1472.